ARMY RESEARCH LABORATORY

ARL

Flow Regime Transition in Inner Grooved Minichannel Cold Plates for Cooling Hybrid Electric Power Electronics

by Darin J. Sharar, Nicholas R. Jankowski, and Avram Bar-Cohen

NOTICES

Disclaimers

The findings in this report are not to be construed as an official Department of the Army position unless so designated by other authorized documents.

Citation of manufacturer's or trade names does not constitute an official endorsement or approval of the use thereof.

Destroy this report when it is no longer needed. Do not return it to the originator.

Army Research Laboratory

Adelphi, MD 20783-1197

ARL-TR-6170   **January 2013**

Flow Regime Transition in Inner Grooved Minichannel Cold Plates for Cooling Hybrid Electric Power Electronics

Darin J. Sharar, Nicholas R. Jankowski, and Avram Bar-Cohen
Sensors and Electron Devices Directorate, ARL

REPORT DOCUMENTATION PAGE

1. REPORT DATE *(DD-MM-YYYY)*	2. REPORT TYPE	3. DATES COVERED *(From - To)*
January 2013		

4. TITLE AND SUBTITLE	5a. CONTRACT NUMBER
Flow Regime Transition in Inner Grooved Minichannel Cold Plates for Cooling Hybrid Electric Power Electronics	5b. GRANT NUMBER
	5c. PROGRAM ELEMENT NUMBER

6. AUTHOR(S)	5d. PROJECT NUMBER
Darin J. Sharar, Nicholas R. Jankowski, and Avram Bar-Cohen	5e. TASK NUMBER
	5f. WORK UNIT NUMBER

7. PERFORMING ORGANIZATION NAME(S) AND ADDRESS(ES)	8. PERFORMING ORGANIZATION REPORT NUMBER
U.S. Army Research Laboratory ATTN: RDRL-SED-E 2800 Powder Mill Road Adelphi, MD 20783-1197	ARL-TR-6170

9. SPONSORING/MONITORING AGENCY NAME(S) AND ADDRESS(ES)	10. SPONSOR/MONITOR'S ACRONYM(S)
U.S. Army TARDEC 6501 E 11 Mile Rd, Bldg 212 Warren MI 48397-5000	11. SPONSOR/MONITOR'S REPORT NUMBER(S)

12. DISTRIBUTION/AVAILABILITY STATEMENT

Approved for public release; distribution unlimited.

13. SUPPLEMENTARY NOTES

14. ABSTRACT

Forced flow of fluids undergoing phase change in traditional single-phase cold plates is an effective way to manage waste heat removal of vehicle power electronics. Such cold plates come in a variety of standard styles, ranging from circular-tubed cold plates and flat-tube cold plates, to more exotic designs such as louvered and offset fin cold plates. The mechanisms of heat transfer in a two-phase system are different than single-phase, and as such, improvement can be made by custom designing cold plates for two-phase operation. Past research has focused on surface modifications that enhance nucleate boiling, convective vaporization, or both during two-phase operation. The method that has gained the most attention is the use of inner grooved tubes for performance improvement in refrigeration applications. Despite the popularity of inner grooved tubes, the flow mechanisms that deliver performance enhancement are not fully understood. The absence of phenomenological insights and physical models makes it difficult to transition inner grooved tube technology from conventional refrigeration equipment to cold plates. Therefore, understanding the physical mechanisms underpinning two-phase performance enhancement in inner grooved tubes is at the heart of this report.

15. SUBJECT TERMS

16. SECURITY CLASSIFICATION OF:			17. LIMITATION OF ABSTRACT	18. NUMBER OF PAGES	19a. NAME OF RESPONSIBLE PERSON
a. REPORT	**b. ABSTRACT**	**c. THIS PAGE**	UU	30	Darin J. Sharar
Unclassified	Unclassified	Unclassified			19b. TELEPHONE NUMBER *(Include area code)* (301) 394-3763

Contents

List of Figures

List of Tables

1. Background

The last several decades have witnessed a dramatic increase in the use of electronics on a vast variety of systems. This trend continues today in hybrid electric vehicle (HEV) and electric vehicle (EV) technologies for commercial and military applications. Military use can include both direct vehicle applications, such as propulsion, and indirect applications, such as electrically operated arms or interfacing with the vehicle electrical system to create a military base microgrid (*1*).

There are several motivations for replacing the traditional internal combustion (IC) motors and mechanical drives with HEV equivalents on military platforms. One of the most important reasons is the high cost of fuel. Transporting fuel to the theater through dangerous routes and over long distances to geographically dispersed troops leads to significant increases in the cost of fuel. The cost can rise from a regular price of several dollars per gallon for civilians to about $400 in the battlefield. If an airlift is needed, the cost can reach $1000 per gallon (*2*). As such, even a modest saving in fuel can lead to huge cost savings on the order of billions of dollars per year.

An additional issue in military vehicle applications is acoustic and heat signature noise, which can be detected by the enemy. A HEV platform can significantly reduce noise and, as a result, improve stealth capabilities and personnel safety in dangerous environments. Furthermore, HEVs can be designed with one motor per axle or even hub motors in each of the wheels for propulsion. This provides the added benefit of system redundancy so that the vehicle can operate in a degraded mode to reach a safe location in case one of the motors fails.

An indirect benefit of HEVs for military applications is the ability to connect multiple HEVs to provide utility-level voltages to bases and other infrastructures in combat zones. With appropriate control electronics, several HEVs can form a microgrid with a robust source of utility power (*1*). This use of HEVs can reduce the need for ancillary generators and power units, therefore leading to savings stemming from acquisition and transportation costs.

1.1 Power Requirements and Power Conversion Electronics

Figure 1 illustrates the continuous power needs for current commercial HEVs, full EVs, and plug-in hybrid electric vehicles (PHEVs). As shown, continuous power demands increase through the transition from commercial HEVs to PHEVs and all-electric drive applications, such as fuel cells or electric vehicles. In the case of HEVs and PHEVs, electrical power requirements approach 30–60 kW, while the all-electric platforms top out around 100 kW for short durations.
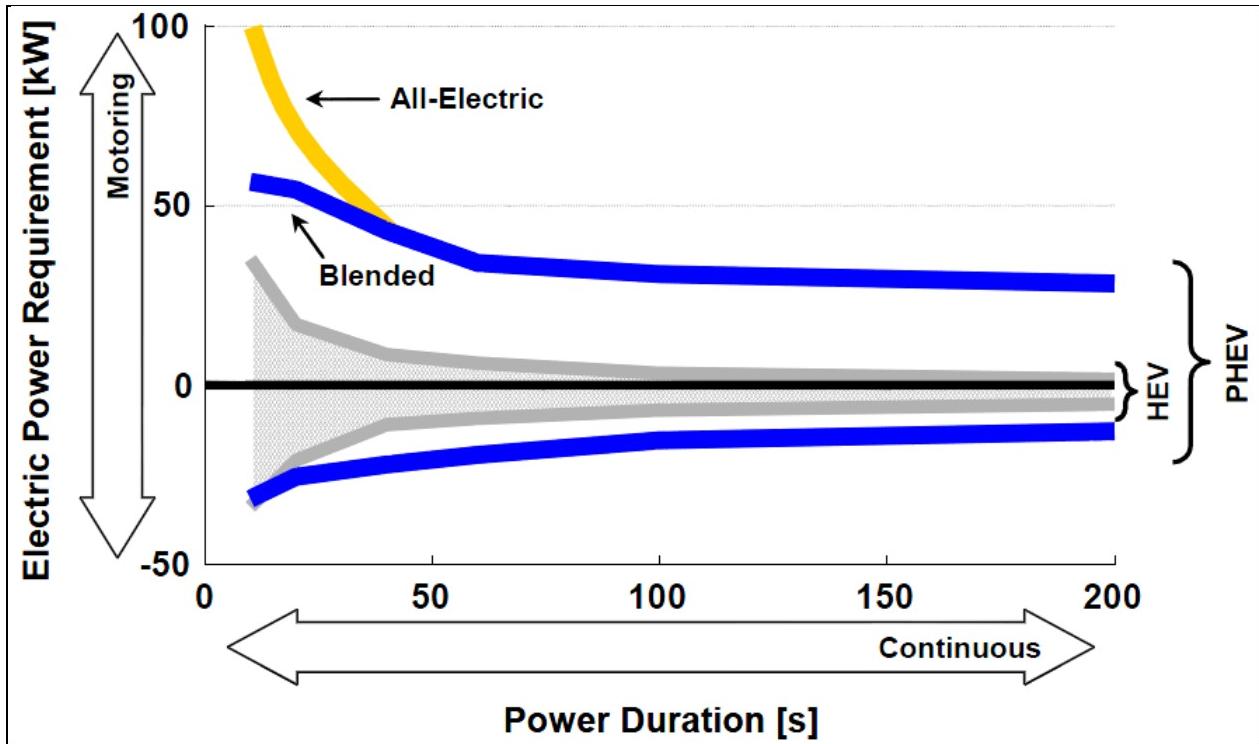
Figure 1. Midsize hybrid electric power requirements (*3*).

A key enabling technology for the transition from traditional gasoline IC engines to hybrid and full electric vehicles is power electronics. Because the disparate electrical systems common to these programs need to draw from a platform's common electrical bus, they all require power conversion electronics to meet operational specifications. This mainly involves the use of power semiconductor switches such as power diodes, metal oxide field effect transistors (MOSFETs), and insulated gate bipolar transistors (IGBTs). Power converters are typically classified by their input and output and, since AC and DC power are possible, there are four types of power converters: DC-DC converter, DC-AC inverter, AC-DC rectifier, and AC-AC converter.

Aligned efforts aimed towards increasing power while simultaneously decreasing power electronic unit size and weight have led to improvements in cost and power density. As shown in table 1, the Department of Energy (DOE) and commercial sectors are targeting a 60% cost reduction, 30% specific power improvement, and 50% power density improvement by 2020. This analysis, although done for a commercial vehicle, is equally applicable to military applications.

Table 1. Status and approximate technical targets for power electronics (*3*).

	R&D Status	Targets	
	2010[a]	2015[b]	2020[b]
Cost, $/kW	<7.9	<5.0	<3.3
Cost, kW/$	>0.127	>0.200	>0.303
Specific power, kW/kg	>10.8	>12.0	>14.1
Power density, kW/L	>8.7	>12.0	>13.4

a. Based on a maximum coolant temperature of 90°C
b. Based on a maximum coolant temperature of 105°C

1.2 Power Electronic Thermal Management

Even with power electronic conversion efficiencies of 96–98%, a vehicle system requiring 100 kW of electrical power would have losses of 2–4 kW. If a system has multiple powertrain motors, high-power bidirectional DC-DC converters, and appropriate power electronics, heat generated in the vehicle system could be significant (*1*). The major concern for thermal management of power electronics is the maximum operation temperature of 125 °C for IGBTs. In general, lower die temperature results in lower losses and better electrical performance. As such, the thermal performance of a power electronics module is determined by the die temperature rise at a given power dissipation.

Traditionally, electronics have relied on air-cooled heat sinks or liquid-cooled cold plates to manage electronic waste heat. However, the new power dense electronic systems are further increasing waste heat and presenting great challenges to the capabilities of conventional cooling systems; fast, compact IGBT devices would have to dissipate heat fluxes in upwards of 250 W/cm² (*1*). Considering strictly air cooling, the effect of higher heat flux electronics is larger, heavier, costlier heat sinks and fans to compensate for insufficient convective performance. The effect is equally dramatic with single-phase liquid cooling, with higher heat fluxes requiring larger coolant flow rates to sufficiently cool the system devices (*4*). These large flowrates and subsequent pumping powers result in increasingly bulky, heavy systems that consume more fuel (*5*). Thus, there is a drive to develop improved cooling components that are smaller and lighter, and have increased performance relative to conventional liquid cold plates.

Cooling schemes using liquid-vapor phase change (two-phase cooling) have been examined as a practical and cost-conscious next step beyond single-phase cooling. A two-phase cooling system has several potential benefits over a standard single-phase liquid cooling approach. First, the latent heat of vaporization for a particular fluid, reflecting the heat absorbed to evaporate a unit mass, can be two orders of magnitude larger than the specific (sensible) heat used in single-phase liquid cooling (*6*). Therefore, boiling provides the possibility of increased heat absorption per

3

unit mass and volume of fluid and improved heat acquisition effectiveness. The single-phase heat dissipation relationship for water can be expressed as:

$$q = \dot{m}C_p dT = \dot{m} \times 4186 \times 20 \sim \dot{m} \times 84000, \qquad (1)$$

where q is the heat dissipation, $\dot{m}$ is the mass flowrate, C_p is the specific heat of the fluid (4186 kJ/kgK for water), and ΔT is the temperature rise of the fluid. Equation 1 assumes an allowable fluid temperature rise of 20 °C, such that the heat dissipation can be expressed as the product of mass flowrate and a constant. Similarly, the two-phase heat dissipation relationship for water can be expressed as:

$$q = \dot{m}h_{lg}x = \dot{m} \times 2257000 \times 0.5 \sim \dot{m} \times 1130000, \qquad (2)$$

where q is the heat dissipation, x is the quality (fraction of the mass flow rate that has been vaporized), $\dot{m}$ is the mass flowrate, and h_{lg} is the latent heat of vaporization of the fluid (2,257 kJ/kg for water). Assuming a moderate exit quality of 0.5, this heat dissipation can also be expressed as the product of the flowrate and a constant. A comparison between equations 1 and 2, with reasonable operating conditions, shows that two-phase has the potential to dissipate an order-of-magnitude more heat than the single-phase case for equivalent flowrates.

As shown symbolically in equations 1 and 2, and graphically in figure 2, the increased heat acquisition effectiveness of two-phase flow translates into lower flowrates compared to single-phase flow for comparable heat dissipation. The potential benefit of lower flowrates includes: smaller fluid reservoirs; smaller onboard fluid volume; reduction in pumping power; smaller pumps; and a reduction in system weight and volume. Additionally, two-phase cooling has the potential benefit of a relatively isothermal cold plate surface, due to the use of latent heat absorption, which occurs at nearly isothermal conditions (7, 8), and order-of-magnitude larger heat transfer coefficients than equivalent single-phase forced convection methods (6, 8).
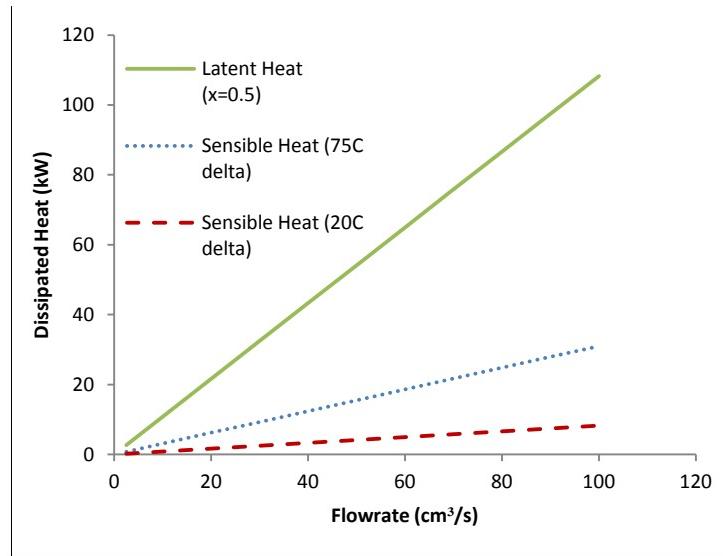
Figure 2. Dissipated heat vs flowrate for water using latent heat and sensible heat (8).

4

2.   Two-Phase Flow Boiling

As shown by Sharar et al. (*8*) and Saums (*7*), performance improvement can be accomplished by simply taking an existing single-phase system, an IGBT minichannel cold plate for cooling power electronics and operating it in two-phase. However, by understanding the mechanisms that make two-phase advantageous, surface enhancements can be developed that work particularly well for two-phase cooling applications. Essential to this understanding is the concept of two-phase flow regime. The remainder of this report will discuss flow regimes in minichannels and introduce passive two-phase surface enhancement techniques. The discussion focuses on single tubes and channels that represent a minichannel cold plate "unit cell." The cold plates could take a variety of forms; the easiest transition, however, may be to integrate the enhanced tubes in a pressure-fit serpentine brazed cold plate. An example of this cold plate design is shown in figure 3.
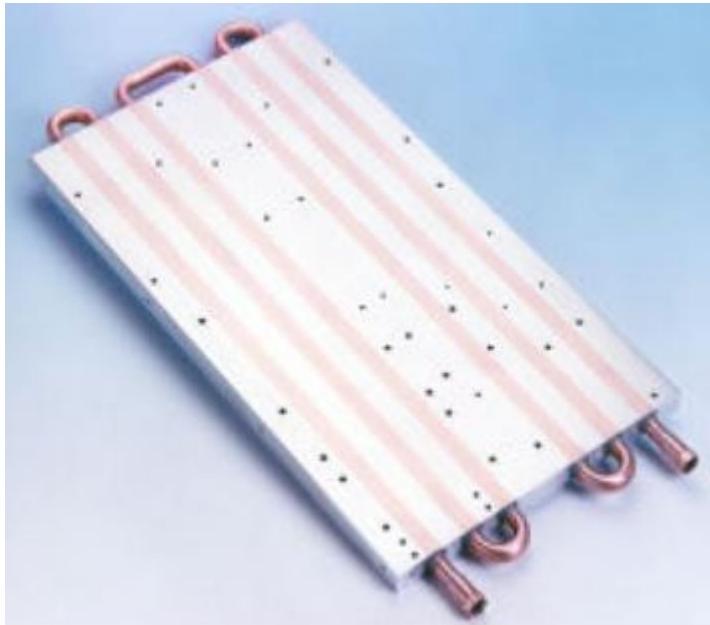
Figure 3. Hydroblok pressure-fit 6-pass serpentine cold plate (*9*).

2.1   Two-phase Flow Regimes

In two-phase flow, the vapor and liquid phases are in simultaneous motion inside the channel or pipe. The physics involved are typically more complicated than single-phase flow. In addition to the viscous, pressure, and inertial effects existing in single-phase flow, two-phase flows are also affected by wall wetting characteristics of the liquid on the channel wall, momentum exchange between the liquid and vapor phases, and interfacial tension forces. The particular flow regime resulting from these interactions plays a critical role in the local heat and mass

transfer. As indicated in equation 3, the two-phase heat transfer coefficient in a closed channel is a summation of the nucleate boiling and convective vaporization terms:

$$h_{tp} = h_{nb} + h_{cv} \tag{3}$$

Understanding these effects in plain tubes is an essential foundation for understanding performance of enhanced channels. Figure 4 is a schematic representation of a typical flow boiling process in a horizontal round tube. The fluid enters as single-phase saturated fluid. As the process proceeds down the length of the tube, the percentage of the flow that has been vaporized increases. Conservation of mass dictates that as the mean density of the flow decreases, due to the formation of vapor, the mean flow velocity must increase. The accompanied acceleration of the flow results in varying liquid and vapor velocities, which causes a series of changes in the flow regime. In other words, the two-phase flow regime is strongly dependent on the relative velocities of the two phases.
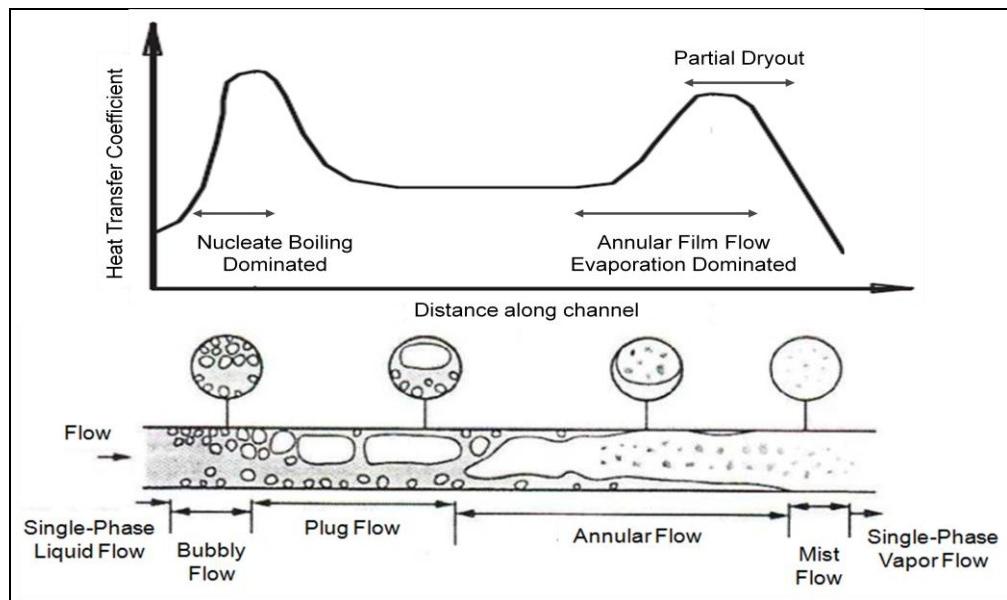
Figure 4. Two-phase flow regimes and associated heat transfer coefficients (*10*).

At low quality, bubbly flow is often observed, where bubbles tend to flow mainly in the top of the tube due to buoyancy forces. In this regime, nucleate boiling is the dominant vaporization mechanism. The added turbulence and mixing resulting from the bubble formation results in a local maximum in the heat transfer coefficient. As the quality downstream increases, bubbles begin to coalesce and larger plugs of vapor form. Like bubbly flow, plugs of vapor tend to flow in the top of the channel due to buoyancy. In this regime, the tube wall is intermittently cooled by liquid slugs and vapor plugs, resulting in a decrease in the heat transfer coefficient. At very low flow rates, stratified flow may occur where the upper portion of the tube is completely occupied by vapor and the bottom by liquid. Stratified flow is marked by drastically reduced

heat transfer coefficients due to the dry upper surface. If the flow rate or quality is increased in stratified flow, Helmholtz instabilities lead to wavy flow and eventually slug flow.

At high vapor velocities, annular flow is observed where a thin liquid film is distributed along the perimeter of the tube and a high-velocity vapor core travels through the center. In the annular flow regime, evaporation from the liquid-vapor interface is the dominant heat transfer mechanism, and the second local maximum in figure 4 is observed. Buoyancy effects may thin the liquid film on the top of the tube and thicken it at the bottom; however, at acceptably high vapor velocities, strong shear stresses serve to redistribute the fluid more evenly around the perimeter of the tube. The strong shear may also lead to entrainment of liquid droplets in the vapor core. Entrained droplets along with continual vaporization tend to thin the liquid film and increase the heat transfer coefficient. Eventually, however, the film may completely disappear from portions of the tube wall. This is known as dryout or critical heat flux (CHF) and causes a decrease in the heat transfer coefficient. As shown in figure 4, gravity tends to cause the film on the top surface to dryout first.

2.2   Flow Regime Maps

The dependence of heat transfer performance on flow regime led researchers to analytically describe and map the dominant flow regimes in channels. Baker (*11*) provided the earliest empirical flow regime map, and other generalized flow regime maps followed—Mandhane et al. (*12*), Taitel and Dukler (*13*), and Weisman et al. (*14*). Most notable among these was the phenomenological maps by Taitel and Dukler, which defined and mapped four adiabatic flow regimes, stratified, intermittent, bubbly, and annular, with superficial liquid and gas coordinates. In 1990, the Unified Model was developed to predict the adiabatic flow regime in a variety of channel sizes and orientations based on two-phase non-dimensional groupings (*15*). These physics-based models contain little empirical fitting and should theoretically apply to most fluids and channel sizes.

Adiabatic models do not account for thermal interactions inside the channel. This is important to consider in diabatic electronic cooling applications where heat is typically added to the two-phase mixture. Specifically, diabatic conditions could be expected to shift transition boundaries between bubbly/intermittent and stratified/intermittent regimes (*16*). As a result, diabatic flow regime maps have been developed to account for the thermal interactions inside of the channel. Beginning in 1998, Kattan, Thome, and Favrat (*17*) empirically modified the Steiner map, which is a modification of the Taitel-Dukler map, and introduced a method for determining the onset of dryout during annular flow in a diabatic system. Since then, other empirically modified diabatic flow regime maps have followed—Zurcher, Thome, and Favrat (*18*), Zurcher, Favrat, and Thome (*19*), Thome and El Hajal (*20*), and Wojtan, Ursenbacher, and Thome (*21*). These modifications provide a more-accurate prediction of the flow regimes and dryout in real-world diabatic systems.

2.3 Studies of Flow Regimes and Flow Regime Maps

The aforementioned models are well established for predicting flow regimes in macroscale channels (D>0.5"). Cheng et al. (*10*) gives a comprehensive review of studies in macroscale smooth channels and provides a summary of results for 24 papers. However, two-phase flow in small diameter channels has become important for compact cold plate applications because of their increased effectiveness, volume reduction, and overall performance improvement when compared to conventional channels. Therefore, it is equally important to discuss flow regime maps in context of mini- and microscale channels.

In general, the empirically modified diabatic flow regime maps discussed previously do not suitably predict flow regimes in micro- and minichannels. As such, new diabatic flow regime maps for flow boiling in micro- and minichannels have been developed (*22–27*). However, the mechanistic model of Taitel-Dukler is in good agreement with a variety of microchannel results from Bar-Cohen and Rahim (*28*), Rahim et al. (*29*), and Triplett et al. (*30*). In addition to demonstrating first-order accuracy in numerous studies, the Taitel-Dukler model has also proven useful for diabatic conditions (*31, 32*). As a consequence, the physics-based model proposed in the Taitel-Dukler flow regime map appears to be appropriate for determining the flow regime during evaporation in various tube diameters.

Recently, Ullmann and Brauner (*33*) studied the effect of tube diameter on the prevailing adiabatic flow regimes in 1.097 mm Pyrex tubes using the experimental data from Triplett et al. (*30*). Ullmann and Brauner indicated the importance of the non-dimensional Eotvos number on the flow regime transition in small tubes. They suggested that by reducing the tube diameter, the stratified region shrinks significantly, and slug, bubbly, and annular flow are the dominant regimes observed. This description of flow regime in mm-sized channels is supported by the aforementioned flow boiling studies in micro- and minichannels, particularly the study by Rahim et al. (*29*), and also consistent with trends predicted by the Taitel-Dukler flow regime maps. Figure 5 shows flow regime maps for R113 flowing in channels with diameters ranging from 100 mm to 0.1 mm, along with mass fluxes from 50 to 400 kg/m²s and qualities from 0.01 to 0.9. As shown, the result of smaller diameter tubes is a gradual expansion of the annular flow regime to lower superficial liquid and vapor velocities, and transition of the bubbly and intermittent flow regimes to lower superficial liquid velocities. Although the primary two-phase flow regimes observed in macroscale channels are also encountered in mini- and microscale channels, annular flow becomes the dominant flow regime as diameter decreases. In the context of inner grooved tubes, it is likely that similar trends exist when transitioning from large diameter macroscale tubes to smaller tubes for compact cold plates of interest in this study.
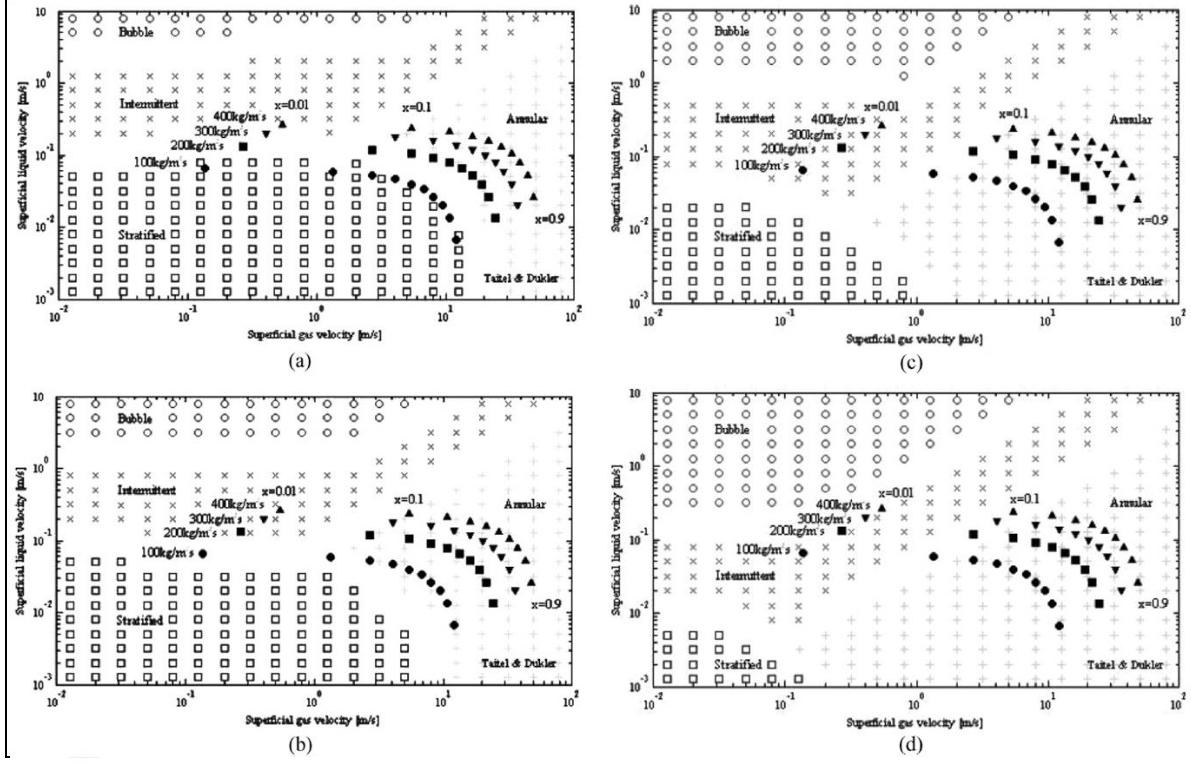
Figure 5. Taitel-Dukler flow regime maps for R113 flowing in a horizontal channel of various diameters (a) 100 mm, (b) 10 mm, (c) 1 mm, and (d) 0.1 mm (*28*).

3. Two-phase Surface Enhancements

Based on an understanding of the flow progression in tubes and the dominant factors affecting the two-phase heat transfer coefficients discussed in chapter 2, researchers have developed surface enhancements to improve thermal performance. Extensive surveys on this topic are reported by Bergles (*34, 35*), Thome (*36*), Webb (*37*), and Kandlikar (*38*). Specific to flow boiling heat transfer, these techniques can be classified into two distinct categories, (1) nucleate boiling techniques, which provide improvement in the first term of equation 3 and an increase in the first local maxima in figure 4 at low vapor qualities; and (2) convective vaporization techniques, which provide improvement in the second term of equation 3 and an increase in the second local maxima in figure 4 at high vapor qualities. A summary of these techniques can be found in table 2 and are discussed extensively in the previous surveys. Furthermore, a closer look at specific topics, including microporous coatings (*39*), reentrant cavities (*40*), nanoparticle fluid additives (*41*), twisted tape inserts (*42, 43*), corrugated tubes (*42, 44*), and inner grooved tubes, can be found in a presentation by Sharar et al. (*45*).

9

Table 2. Classification of flow boiling enhancement techniques.

Nucleate Boiling	Convective Vaporization
Acoustic pulsation	Fins
Mechanical and ultrasonic vibration	Twisted tape inserts
Porous surfaces	Helical wire inserts
Structured surfaces (reentrant cavities)	Corrugated or fluted tubes
Screens	Inner grooved tubes (microfin tubes)
Fins	
Electrohydrodynamic field effect	

3.1   Convective Vaporization

In order to take full advantage of a two-phase cooling scheme and the flowrate/pumping power benefits of latent heat transfer, a large percentage of fluid should be vaporized. As such, operation beyond the first maximum, where nucleate boiling is likely suppressed and convective vaporization dominates, is of particular interest. Not surprisingly, there are a variety of convective vaporization enhancements that have been explored deeply in academic settings and others that have been adopted commercially in refrigeration applications. The three main convective vaporization enhancement techniques that have been commercially adopted to improved tube-side performance of refrigeration tubes are twisted tape inserts, corrugated tubes, and inner grooved tubes.

3.1.1 Inner Grooved Tube

Twisted tape inserts and corrugated tubes have been commercially available for many years; both, however, have been largely displaced by inner grooved tubes. Inner grooved tubes were originally developed in Japan and gained widespread adoption in the 1980s (*42*). Seamless inner grooved tubes are typically manufactured by running a mandrel through a smooth bore copper tube but can also be made by embossing fin geometries on a metal strip, rolling, and seam welding. The latter manufacturing method provides a wider range of microfin geometries, including 3-D geometries, but most commercial vendors continue to manufacture seamless tubes (*46*). Figure 6a shows the characteristic inner grooved tube geometry, which is defined by the internal diameter, number of fins, helix angle β (or axial pitch), fin height, fin angle γ, and the internal area ratio. Figure 6b shows a photograph of a commercial Wieland Cuprofin inner grooved tube along with appropriate geometric parameters.
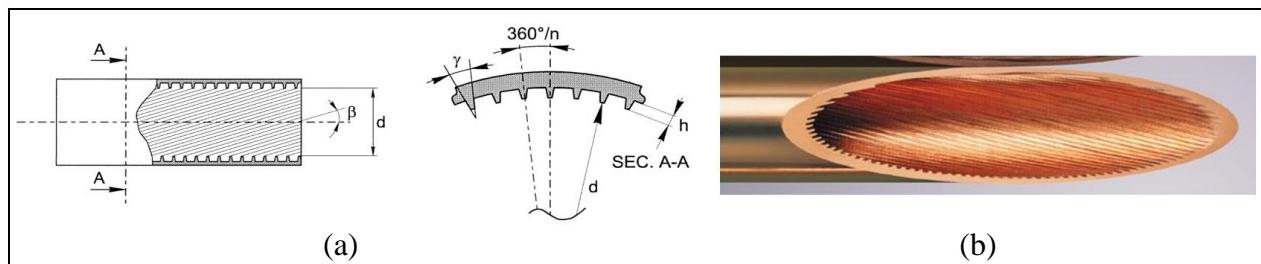

Figure 6. (a) Schematic of inner grooved tube and (b) Photograph of inner grooved tube (courtesy Wieland).

Depending on the process, tube size, and manufacturer, the enhancement typically consists of 40–80 small ~0.1 to 0.4 mm tall fins with helix angles from 7° to 23°. The majority of inner grooved tubes have fins with approximately trapezoidal cross-sectional shapes, but triangular and rectangular fins are also possible. Table 3 lists geometric parameters for three commercially available inner grooved tubes from Wieland.

Table 3. Geometric parameters and fin efficiencies for three Wieland inner grooved tubes,

Name	Diameter (mm)	Wall thickness (mm)	# fins	Fin Height (mm)	Approximate Fin base (mm)	ηf (%) h=1000 W/m²	ηf (%) h=20,000 W/m²	Surface enhancement (A/Ap)
S2AD-5	5	0.23	40	0.15	0.20	99	98	1.52
S2AD-952	9.52	0.34	60	0.2	0.25	99	97.5	1.52
S2AD-15	15	0.4	75	0.3	0.31	99	96.7	1.53

As tabulated in table 3, the resulting fin efficiencies are greater than 95% for all three tubes, with heat transfer coefficients ranging from 1,000–20,000 W/m²K. Furthermore, the curves for triangular, rectangular, and parabolic fins converge at $L_c^{3/2}\left(h/kA_p\right)^{1/2}$ values less than 0.3, which suggests that fin profile does not significantly affect fin efficiency in standard inner grooved tubes (*47*).

In horizontal orientations, inner grooved tubes typically show heat transfer enhancement ratios as high as three to four times at low mass velocities and improvement equal to or greater than the internal area ratio at high mass velocities (*42*). For vertical applications, heat transfer enhancement less than or equal to horizontal applications can be expected. Pressure drop increase compared to a smooth tube is typically small, ranging from 1.0 at low mass velocities to 1.5 at high mass velocities. From a heat transfer versus pressure drop perspective, inner grooved tubes outperform twisted tape inserts and corrugated tubes. Heat transfer improvement and pressure drop increase for each of the three enhancement technologies are compiled in table 4.

Table 4. Comparison of leading refrigeration tube performance (*42*).

Metric	Microfin Tube	Twisted Tape Insert	Corrugated Tube
Heat Transfer Augmentation @ low mass flux	3 to 4x that of a plain tube	1.2 to 1.5x that of a plain tube	1.2 to 1.8x that of a plain tube
Heat Transfer Augmentation @ high mass flux	≥ internal area ratio	1.2 to 1.5x that of a plain tube	Close to microfin tube performance
Pressure Drop Penalty	1 to 1.5x that of a plain tube	2x that of a plain tube	2x that of a plain tube

3.1.2 Heat Transfer Mechanisms in Inner Grooved Tubes

Despite widespread use and demonstrated performance improvement, the mechanisms leading to enhanced performance in inner grooved tubes are not well understood. Subsequently, there is a lack of physical models to predict performance in inner grooved tubes, which makes

transitioning from conventional refrigeration equipment to cold plates difficult. Therefore, understanding the physical mechanisms underpinning two-phase performance enhancement in inner grooved tubes is a critical bottleneck.

Since the 1980s, a variety of studies have been performed to demonstrate and determine the enhancement mechanisms. In one example, Kim and Shin (*48*) performed an extensive experimental flow boiling study with R22 and R410A in one 9.52 mm OD (8.70 mm ID) smooth tube, five 9.52 mm OD (8.46–8.68 mm ID) inner grooved tubes, and two 9.52 mm OD (8.14– 8.51 mm ID) cross grooved tubes. The geometric parameters of interest and results summary are shown in table 5. As shown in the second-to-last column, the area enhancement (A/Ap) for each of the five inner grooved tubes varied from 1.28 to 1.85. The last column shows the average heat transfer coefficient for each fluid tested, with a mass flow rate of 205–215 kg/m²s, heat flux of 11 kW/m², and quality ranging from 0.2 to 0.85. Similar to other studies (*49–51*), a comparison of the area enhancement ratio to the heat transfer enhancement shows that inner grooved tubes provide enhancement greater than the area enhancement alone at moderate to low mass flux. These results are consistent with the trends discussed in table 4.

Table 5. Specifications of smooth and inner grooved tubes tested, area enhancement ratios, and average heat transfer enhancement ratios for mass flow rates ranging from 205–215 kg/m²s, heat flux of 11 kW/m², and quality ranging from 0.2 to 0.85.

Tube types		Fin profile	D_i (mm)	D_{ai} (mm)	T (mm)	W_t (mm)	H_f (mm)	β (°)	α (°)	Number of fins	H_f/D_i	A/A_p	$\eta_h = h/h_{smooth}$	
													R22	R410A
Smooth tube	ST	Smooth	8.70	8.70	0.41	0.41	–	–	–	–	–	1.0	1.00	1.00
Single-groove	MF-1		8.68	8.82	0.30	0.35	0.12	25	–	60	0.0138	1.28	1.86	1.93
	MF-2		8.52	8.80	0.30	0.36	0.20	18	53	60	0.0235	1.51	2.00	2.04
	MF-3		8.52	8.80	0.30	0.36	0.20	18	40	60	0.0235	1.60	2.98	2.33
	MF-4		8.47	8.80	0.28	0.36	0.25	15.5	25	65	0.0295	1.85	3.27	2.99
	MF-5		8.46	8.80	0.30	0.36	0.23	30	40	54	0.0272	1.53	2.24	2.02

Researchers have speculated that the improvement beyond area enhancement is a result of several factors: thinning of liquid film in annular flow due to the larger surface area (*48*), redistribution of liquid in annular flow due to the helical grooves (*52*), and increased turbulence. However, generalized models that attempt to capture these effects have proven unreliable. Other research has suggested that flow regime transition (*50, 51*) and delay of dryout at high vapor qualities due to groove-induced fluid redistribution (*53*) appear to be two leading enhancement mechanisms (and benefits) of inner grooved tubes. To one degree or another, all of these mechanisms likely play a role in the enhanced performance in inner grooved tubes; however, the focus of the following sections is flow regime transition and delay of dryout.

3.1.3 Flow Regime Transition and Delayed Dryout in Inner Grooved Tubes

As previously discussed, the particular flow regime in a channel is intrinsically tied to the heat transfer performance. Therefore, transition from an undesirable flow regime, such as stratified flow (where only the bottom portion of the tube is wetted), to a desirable flow regime, such as annular flow (where thin film evaporation around the periphery leads to high heat transfer

coefficients), could result in significant improvement. In this context, understanding flow regimes typical in inner grooved tubes relative to smooth tubes, and the effect of tube diameter on performance, is a key component to the successful transition to cold plate form factors.

The suggested link between flow regime and thermal performance is not a broadly accepted approach, but there is empirical and analytical evidence suggesting that this approach to explaining enhancement in inner grooved tubes is appropriate. In one example, Yu, Lin, and Tseng (*50*) performed a flow visualization and heat transfer study with R134a in a 10.7 mm ID smooth and an 11.1 mm ID inner grooved tube. Mass fluxes in the range of 163 to 408 kg/m²s, heat flux between 2,200 and 56,000 W/m², and a fixed heated length of 1.5 m were tested. Figure 7 shows the results of the flow visualization, plotted in the coordinates of G (mass flow rate) and x (quality); figure 7a is the smooth tube experimental results and figure 7b is the inner grooved tube results. The transitions of flow pattern observed were wavy, intermittent, semi-annular, and annular in the direction of increasing G and x. It was reported in the study, and also apparent from figure 7, that the transitions in the inner grooved tube occurred at lower G and x compared with the smooth tube. Under the same flow conditions, the flow pattern in the inner grooved tube transitioned to annular flow, while the smooth tube was still operating in the wavy flow regime. One clear example is at a mass flowrate of G=163 kg/m²s and a quality of x>0.3.
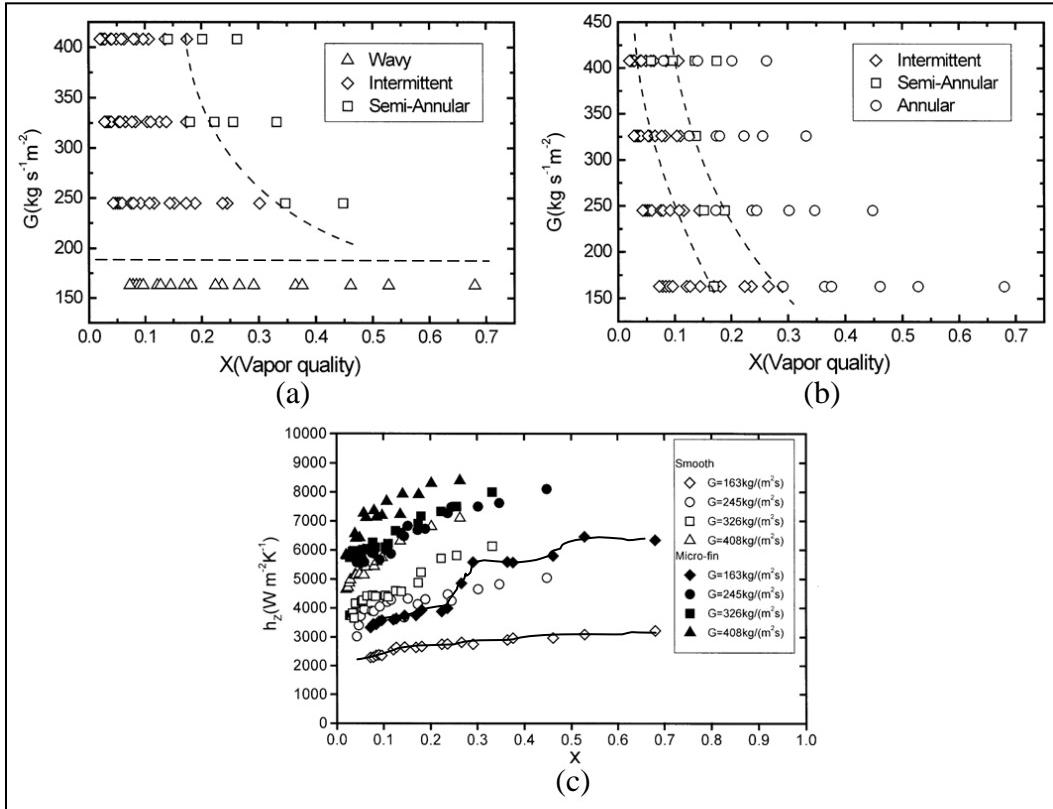

Figure 7. Experimental flow regime maps for (a) smooth tube with 10.7 mm ID, (b) inner grooved tube with 11.1 mm ID, and (c) average heat transfer coefficient for the smooth and inner grooved tube.

The earlier transitions in the inner grooved tube are a result of the helical grooves on the tube surface, which allow liquid to more easily reach the top portion of the tube. In the smooth tube, however, the liquid and vapor velocities have to become sufficiently high before transitions can "naturally" occur. As a result of flow regime transition, the heat transfer is enhanced in the inner grooved tube. Figure 7c shows the average heat transfer coefficient versus vapor quality for the smooth tube and inner grooved tube. It can be seen that the heat transfer coefficient increases with both G and x for the smooth tube and inner grooved tubes. The increase in the heat transfer coefficient is relatively smooth for conditions when the flow regime does not change. One example is the case of G=163 kg/m²s in the smooth tube, where wavy flow dominates; compare figures7a and c. However, the rise can be dramatic where flow pattern transitions occur; from figure 7b, the flow regime transitions from intermittent to annular at a quality of 0.3 and a flowrate of G= 163 kg/m²s. This same condition on figure 7c marks a sharp increase in heat transfer coefficient from approximately 4,000 to 5,500 W/m²K (40% improvement). Consequently, the maximum heat transfer enhancement of 2 occurred at a flowrate of 163 kg/m²s and qualities 0.3<x<0.7, where wavy flow dominated in the smooth tube and flow transition from intermittent to annular in the inner grooved tube was achieved. This enhancement exceeded the reported area enhancement of 1.6. Similar performance improvements were demonstrated by Hatamipour and Akhavan-Behabadi (*51*) during flow boiling of R134a in 8.92 mm ID smooth and inner grooved tubes.

In yet another example, Shedd and Newell (*52*) used a non-intrusive optical film thickness measurement method to observe the liquid distribution in horizontal adiabatic water-air flow through 15.1 mm ID smooth and inner grooved tubes. Liquid film thickness profiles for stratified/annular flow through smooth and 18° helix tubes are shown in figure 8. The smooth tube films are represented by dotted lines, and the grooved tube film thicknesses are shown with solid lines. At low mass flux, 44 kg/m²s, the smooth tube profiles are basically symmetric from left to right, with thicker liquid films on the bottom and dry surfaces at the top surface due to gravity effects; this can be interpreted as stratified flow. The grooved tube profiles appear to be rotated counterclockwise (the same direction as the groove) and the periphery is almost entirely wetted; this can be interpreted as annular flow. Under these flow conditions, 62% of the smooth tube is wetted versus 94% of the 18° inner grooved tubes. The observed transition from stratified to annular flow, leading to a larger wetter perimeter, would almost certainly cause higher heat transfer coefficients and may explain the enhancement in inner grooved tubes. Shedd and Newell (*52*) also reported that the liquid film profiles for the smooth and inner grooved tubes tend to converge at higher mass flux, which provides an explanation for the decrease in enhancement at higher mass flux as seen in the literature and outlined in table 4.
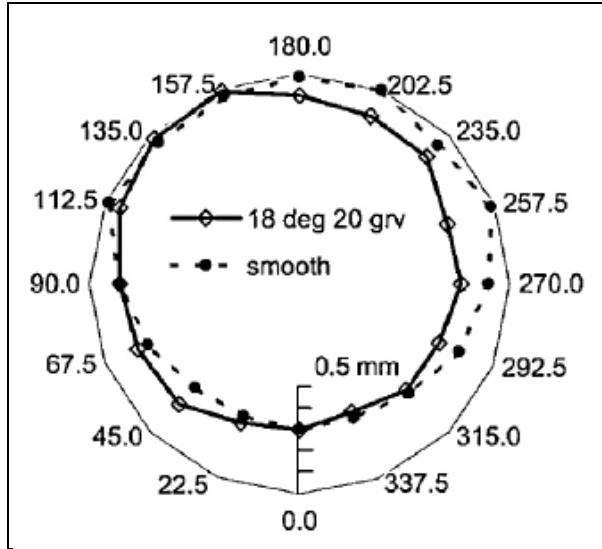
Figure 8. Film thickness profiles for smooth and 18 grooved
tubes with mass fluxes of G=44 kg/m²s and qualities
ranging from 0.6 to 0.76 (*52*).

Honda and Wang (*54*), and Mikishi, Honda, and Wang (*55*) recognized the dependence of heat
transfer on the particular flow regime and, as such, developed stratified and annular flow models
for evaporative heat transfer in inner grooved tubes. In doing so, they modified the flow regime
transition from stratified-wavy to annular flow proposed by Kattan et al. (*17*) to predict the heat
transfer coefficient in the intermediate region between the stratified and annular flow models. In
both the stratified and annular models, nucleate boiling and forced convection were accounted
for (*55*). The predictions of the new theoretical models and previously proposed empirical
models by Koyama et al. (*56*), Murata (*57*), Thome et al. (*58*), Cavallini et al. (*59*), Yun et al.
(*60*), and Mori et al. (*61*) were compared to available experimental data for 10 inner grooved
tubes and four refrigerants. As shown in table 6, the models developed to account for the
dependence of flow regime (labeled Present 1 and Present 2) had smaller rms errors than the
empirical models. The rms errors of the "present" models are still fairly high and improvements
could be made. However, the underlying conclusion remains: heat transfer in inner grooved
tubes appears to be dependent on flow regime (and flow regime transition), and
phenomenological models need to be developed that appropriately reflect this point.

15

Table 6. Error analysis for various inner grooved tube heat transfer coefficient models (*55*).

Tube	Refrigerant	N	Murata		Koyama et al.		Thome et al.		Cavallini		Yun et al.		Mori et al.		Present 1		Present 2	
			am	rms	am	rms	am	rms	am	rms	am	rms	am	rms	am	rms	am	rms
A	R22	37	−28.2	42.7	−7.5	19.8	−18.4	23.4	−52.0	53.0	−48.1	58.3	−34.2	39.0	−7.9	18.1	−12.5	18.8
A	R134a	31	−30.3	36.5	6.5	23.1	−6.2	28.2	−52.9	55.0	−40.9	49.2	−28.6	36.6	−10.9	19.3	−15.2	21.4
A	R123	28	12.5	28.5	−5.1	21.7	41.8	53.0	−39.5	42.4	−15.7	35.6	16.4	31.7	5.7	16.3	−0.8	14.1
B	R410A	22	−47.9	48.5	−19.4	30.3	−26.8	31.3	−46.3	48.2	−67.3	68.2	−31.1	33.5	21.1	26.8	−19.6	22.9
C	R410A	24	−36.3	41.1	−11.6	22.6	−17.0	21.0	−17.7	25.3	−59.3	61.9	−8.1	20.5	14.7	22.3	−5.0	13.9
D	R22	18	−19.2	19.8	23.9	26.7	16.7	17.9	−38.7	39.0	−43.7	46.2	−26.1	26.3	−18.8	19.6	12.6	17.2
E	R22	25	31.7	41.0	28.5	38.9	104.3	111.5	37.6	39.3	−41.0	50.8	123.0	134.1	28.7	38.3	50.4	55.7
F	R22	8	7.0	29.5	−9.3	19.8	49.9	50.3	95.2	95.6	−57.7	60.7	156.0	157.0	−15.9	16.4	15.7	32.8
G	R22	6	−27.1	29.8	−40.8	41.7	4.5	7.6	11.3	16.7	−69.4	69.9	49.2	50.0	−22.5	26.1	−21.8	25.9
H	R22	14	−18.4	25.0	−30.6	32.5	0.6	15.1	29.8	35.8	−68.5	69.4	49.9	62.1	−11.9	18.1	2.3	19.3
I	R22	15	−25.1	30.7	−35.4	37.2	11.6	31.8	30.8	43.7	−71.5	72.4	47.1	67.2	−6.2	11.9	−5.5	11.9
J	R22	6	−12.5	19.3	−29.1	30.7	5.0	6.7	82.2	84.0	−63.3	64.1	125.5	126.0	−15.0	19.3	−2.6	18.1
All data		234	−16.9	36.4	−5.3	27.9	12.1	46.8	−15.7	48.2	−49.1	57.1	16.0	67.0	0.4	22.4	−0.4	25.7

am: arithmetic mean value, rms: root mean square value

The inner grooved tube studies discussed so far have had internal diameters in the range 7–15 mm, and the empirical studies were developed based on tubes this size. Furthermore, no inner grooved tube flow visualization studies below 8.5 mm ID were reported, despite the known dependence of flow regime on tube diameter. In fact, only one study by Dang, Haraguchi, and Hihara (*53*) addressed flow boiling in small inner grooved tubes. In this study, flow boiling heat transfer of carbon dioxide inside a small-sized 2 mm ID inner grooved tube with heat fluxes ranging from 4.5–18 kW/m² and mass fluxes from 360–720 kg/m²s was investigated. As shown in figure 9, the heat transfer coefficients in the inner grooved tubes were 1.88 to 2.2 times larger than the smooth tube values under the same experimental conditions; the area enhancement was close to 2.0 in this study. These trends are consistent with the trends discussed in table 4; heat transfer improvement in inner grooved tubes approaches the area enhancement at high mass fluxes. Despite the modest heat transfer improvement, the dryout quality for the inner grooved tubes was much higher than the smooth tubes, ranging from 0.9–0.95 versus 0.6–0.8, respectively. These experimental results indicate that using small 2 mm ID microfin tubes may considerably increase the overall heat transfer performance and delay dryout in annular flow at high qualities. In the future, an accompanying flow visualization study, lower flowrates to promote stratified flow and observe flow regime transition, and a detailed look at the delay of liquid film dryout in small inner grooved tubes could provide insight.
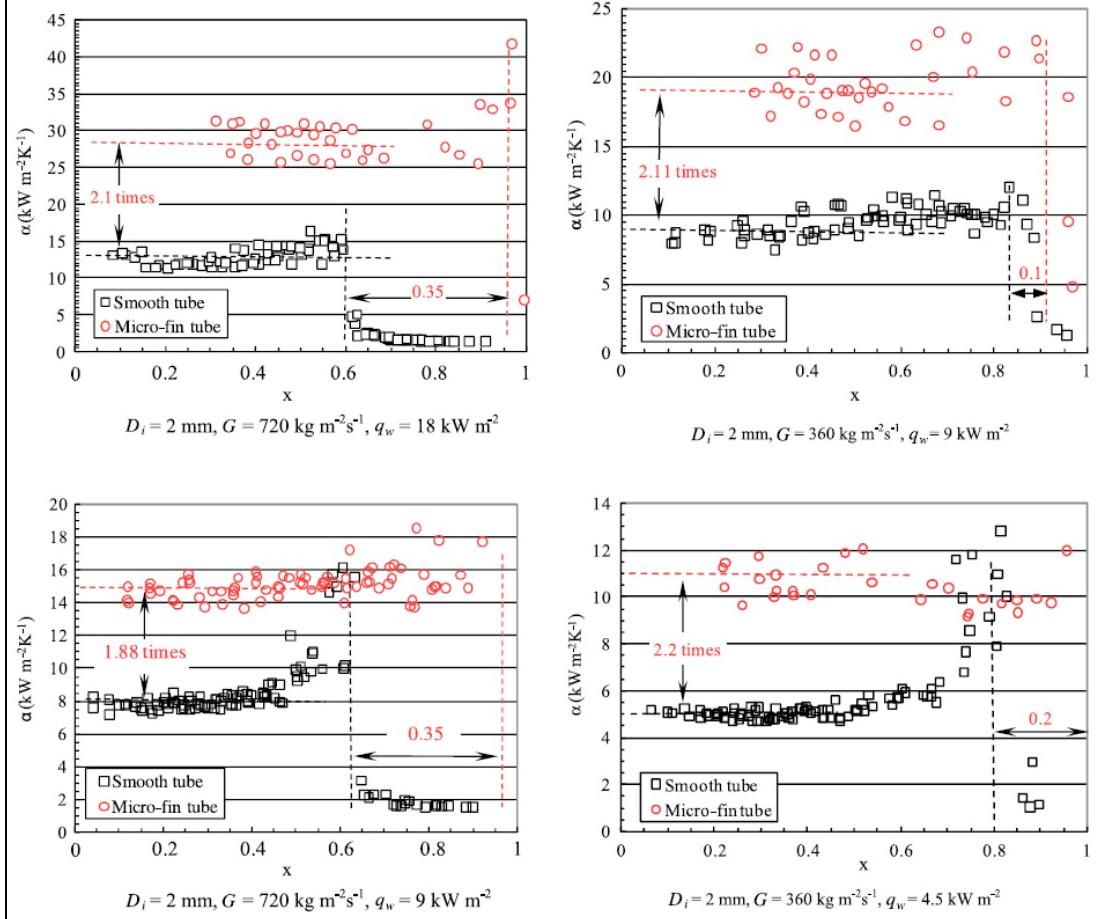
Figure 9. Comparison between heat transfer coefficients of smooth and inner grooved tubes for two different mass fluxes and heat fluxes (*53*).

It is likely that extrapolating empirical correlations to smaller tube diameters will provide inaccurate predictions because, as shown previously, flow regime and heat transfer coefficient changes with tube diameter. In addition, the "present" models (*55, 54*) rely on the modified Kattan et al. (*17*) stratified-wavy to annular flow regime transition, which, as discussed previously, does not suitably predict flow regimes in mini- and microchannels. Finally, Makishi et al. (*55*) combine nucleate boiling and convection in the model to reduce error. While this may be necessary for large tubes where the liquid film is thicker, nucleate boiling likely becomes progressively less important as the diameter shrinks, the quality grows, and thinner films are experienced.

4. Conclusion

Two-phase cooling solutions are being explored to dissipate waste heat associated with next-generation power conversion electronics. Essential to two-phase heat transfer performance is the particular flow regime; annular flow is desirable because it provides high heat transfer coefficients. In standard channels, liquid and vapor velocities have to become sufficiently high before transition into annular flow can occur. Inner grooved tubes, on the other hand, have been shown to demonstrate earlier transition into annular flow and enhanced heat transfer as a result. By incorporating inner grooved tubes into power electronic cold plates, improvement may be obtained.

Flow boiling in smooth tubes (channels) of various sizes has been explored, and adequate physical models predicting flow regime and heat transfer are available. Unfortunately, inner grooved tube flow visualization studies have been limited to tubes ranging in size from 8.62 to 11.1 mm OD, fin angles from 15 to 18°, and fin heights from 0.25 to 0.3 mm with R-134a and CO_2 as the working fluids. There is an apparent lack of inner grooved tube flow visualization data in the literature, and the few studies that have been conducted have not explored a variety of tube diameters and fluids. Therefore, motivation exists to study flow visualization in inner grooved tubes through a spectrum of tube diameters—particularly minichannels and microchannels for cold plate form factors. In addition to contributing valuable data to the scientific community, these studies would provide the data necessary to perform a more complete assessment of flow regime maps for application to inner grooved tubes and improve the communities understanding of the mechanisms leading to enhanced heat transfer in inner grooved tubes. Results obtained from such studies would aid in developing next-generation cold plates incorporating inner grooved tube technologies for enhanced performance.

Bibliography

1. Mi, C.; Masrur, M. A.; Gao, D. *Hybrid Electric Vehicles: Principles and Applications with Practical Perspectives*; West Sussex: John Wiley and Sons Ltd., 2011.

2. Robinson, B. defensesystems.com, 26 February 2010. [Online]. Available: http://www.defensesystems.com/Articles/2010/03/11/Defense-IT-3-Greens.aspx. [Accessed 2 August 2012].

3. U.S. Department of Energy: Energy Efficiency and Renewable Energy, 7 December 2010. [Online]. Available: http://www1.eere.energy.gov/vehiclesandfuels/resources/fcvt_plans_ roadmaps.html. [Accessed 3 August 2012].

4. Garimella, S.; Singhal, V. Single-phase Flow and Heat Transport in Microchannel Heat Sinks. *1st International Conference on Microchannels and Minichannels,* April 2003.

5. Coutteau, C. *Advanced Planning Briefing to Industry (APBI), TARDEC Ground Vehicle Power and Mobility (GVPM)*; U.S. Army RDECOM-TARDEC: Warren, Michigan, October 2008.

6. Mudawar, I. Assessment of high-heat-flux thermal management schemes. *IEEE Transactions on Components and Packaging Technologies* **June 2001***, 24* (2), 122–141.

7. Saums, D. Vaporizable Dielectric Fluid Cooling of IGBT Power Semiconductors for Vehicle Powertrains. *6th International Conference on Integrated Power Electronics Systems,* pp. 437–444, 2010.

8. Sharar, D.; Jankowski, N.; Morgan, B.; Bar-Cohen, A. Two-phase Minichannel Cold Plate for Army Vehicle Power Electronics. *ASME InterPACK* **2011***, 2*, 133–142.

9. Hydroblok Series - Liquid Cooled Cold Plates, D6 Industries, [Online]. Available: http://www.d6industries.com/liquid-cold-plates.html. [Accessed 31 August 2012].

10. Cheng, L.; Ribatski, G.; Thome, J. Two-phase Flow Pattern Maps: Fundamentals and Applications. *ASME Applied Mechanics Reviews* **2008***, 61*.

11. Baker, O. Simultaneous Flow of Oil and Gas. *Oil and Gas Journal* **1954***, 53* (12), 185–195.

12. Mandhane, J.; Gregory, G.; Aziz, K. A Flow Pattern Map for Gas Liquid Flow in Horizontal Pipes. *International Journal of Multiphase Flow* **1974***, 1* (4), 537–553.

13. Taitel, Y.; Dukler, A. A Model for Predicting Flow Regime Transitions in Horizontal and Near Horizontal Gas-liquid Flow. *AiChE Journal* **1976***, 22* (1), 47–55.

14. Weisman, J.; Duncan, D.; Gibson, J.; Crawford, T. Effect of Fluid Properties and Pipe Diameter on Two-phase Flow Pattern in Horizontal Lines. *Internation Journal of Multiphase Flow* **1979**, *5* (6), 437–462.

15. Taitel, Y. Flow Pattern Transition in Two Phase Flow. *Proc. in 9th International Heat Transfer Conference,* pp. 237–254, 1990.

16. Bar-Cohen, A.; Ruder, Z.; Griffith, P. Thermal and Hydrodynamic Phenomena in a Horizontal Uniformly Heated Steam Generating Pipe. *Journal of Heat Transfer* **1987**, *109* (3), 739–745.

17. Kattan, N.; Thome, J.; Favrat, D. Flow Boiling in Horizontal Tubes. Part I: Development of a Diabatic Two-phase Flow Pattern Map. *Journal of Heat Transfer* **1998**, *120* (1), 140–147.

18. Zurcher, O.; Thome, J.; Favrat, D. Evaporation of Ammonia in a Smooth Horizontal Tube: Heat Transfer Measurements and Predictions. *Journal of Heat Transfer* **1999**, *121*, 89–101.

19. Zurcher, O.; Favrat, D.; Thome, J. Development of a Diabatic Two-phase Flow Pattern Map for Horizontal Flow Boiling. *International Journal of Heat and Mass Transfer* **2002**, *45*, 291–301.

20. Thome, J.; El Hajal, J. Two-phase Flow Pattern Map for Evaporation in Horizontal Tubes: Latest Version. *Heat Transfer Engineering* **2003**, *24* (6), 3–10.

21. Wojtan, L.; Ursenbacher, T.; Thome, J. Investigation of Flow Boiling in Horizontal Tubes: Part I - A New Diabatic Two-phase Flow Pattern Map. *International Journal of Heat and Mass Transfer* **2005**, *48*, 2955–2969.

22. Harirchian, T.; Garimella, S. A Comprehensive Flow Regime Map for Microchannel Flow Boiling with Quantitative Transition Criteria. *International Journal of Heat and Mass Transfer* **2010**, *53*, 2694–2702.

23. Revellin, R.; Thome, J. Experimental Investigation of R-134a and R-245fa Two-phase Flow in Microchannels for Different Flow Conditions. *International Journal of Heat and Fluid Flow* **2007**, *28*, 63–71.

24. Hestroni, G.; Mosyak, Z.; Segal, Z.; Pogrebnyak, E. Two-phase Flow Patterns in Parallel Microchannels. *International Journal of Multiphase Flow* **2003**, *29*, 341–360.

25. Huo, X.; Chen, L.; Tian, Y.; Karayiannis, T. Flow Boiling and Flow Regimes in Small Diameter Tubes. *Applied Thermal Engineering* **2004**, *29*, 1225–1239.

26. Revellin, R.; Dupont, V.; Ursenbacher, T.; Thome, J.; Zun, I. Characterization of Diabatic Two-phase Flows in Microchannels: Flow Parameter Results for R-134a in a 0.5 mm Channel. *International Journal of Multiphase Flow* **2006**, *32*, 755–774.

27. Ong, C.; Thome, J. Flow Boiling Heat Transfer of R134a, R236fa, and R245fa in a Horizontal 1.030 mm Circular Channel. *Experimental Thermal Fluid Science* **2009**, *33*, 651–663.

28. Bar-Cohen, A.; Rahim, E. Modeling and Prediction of Two-phase Microgap Channel Heat Transfer Characteristics. *Heat Transfer Engineering* **2009**, *30*, (8), 601–625.

29. Rahim, E.; Revellin, R.; Thome, J.; Bar-Cohen, A. Characterization and Prediction of Two-phase Flow Regimes in Miniature Tubes. *International Journal of Multiphase Flow* **2010**, *37*, 12–23.

30. Triplett, K.; Ghiaasiaan, S.; Abdel-Khalik, S.; Sadowski, D. Gas-liquid Two-phase Flow in Microchannels. Part I: Two-phase Flow Patterns. *International Journal of Multiphase Flow* **1999**, *25*, 377–394.

31. Frankum, D.; Wadekar, V.; Azzopardi, B. Two-phase Flow Patterns for Evaporating Flow. *Experimental Thermal and Fluid Science* **1997**, *15* (3), 183–192.

32. Taitel, Y.; Lee, N.; Dukler, A. Transient Gas-liquid Flow in Horizontal Pipes: Modeling the Flow Pattern Transitions. *AIChE Journal* **1978**, *24* (5), 920–934.

33. Ullmann, A.; Brauner, B. The Prediction of Flow Pattern Maps in Mini Channels," *Multiphase Science Technology* **2007**, *19* (1), 49–73.

34. Bergles, A. Heat Transfer Enhancement - The Encouragement and Accommodation of High Heat Fluxes," *Journal of Heat Transfer* **1997**, *119*, 8–19.

35. Bergles, A. Techniques to Enhance Heat Transfer. in *Handbook of Heat Transfer*, New York, NY, McGraw-Hill, 1998.

36. Thome, J. *Enhanced Boiling Heat Transfer*; Washington, DC: Hemisphere Publishing Corp., 1990.

37. Webb, R. *Principles of Enhanced Heat Transfer*; New York, NY: John Wiley and Sons, Inc., 1994.

38. Kandlikar, S.; Spiesman, P. Augmentation of Saturated Flow Boiling Heat Transfer; in *Chapter 18, Handbook of Phase Change*, Philadelphia, PA, Taylor and Francis, 1999.

39. Moreno, G.; Naramanchi, S.; Thiagarajan, S.; Bennion, K.; Venson, T. Enhanced Surfaces to Improve Power Electronics Cooling. in *MEPTEC*, San Jose, 2011.

40. Yilmaz, S.; Hwalck, J.; Westwater, J. *Pool Boiling Heat Transfer Performance for Commercial Enhanced Tube Surfaces*; ASME Paper 90-HT-41, 1980.

41. Kim, H.; Kim, J.; Kim, M. Effect of Nanoparticles on CHF Enhancement in Pool Boiling of Nano-fluids. *International Journal of Heat and Mass Transfer* **2006**, *49*, 5070–5074.

42. Thome, J. *Chapter 11: Boiling Heat Transfer Inside Enhanced Tubes*; in Wolverine Engineering Data Book III, 2004.

43. Jensen, M.; Bensler, H. Saturated Forced-convection Boiling Heat Transfer with Twisted-tape Inserts. *Journal of Heat Transfer* **1986***, 108*, 93–99.

44. Laohalertdecha, S.; Wongwises, S. An Experimental Study Into the Evaporation Heat Transfer and Flow Characteristics of R-134a Refrigerant Flowing Through Corrugated Tubes. *International Journal of Refrigeration, 34*, 280–291.

45. Sharar, D.; Nicholas, J.; Morgan, B.; Bar-Cohen, A. Enhanced Two-Phase Cooling. in *IMAPS 2012 Chesapeake Chapter*, College Park, MD, 2012.

46. Houfuku, M. Development Trends in Inner-grooved Tubes in Japan. *Hitachi Cable Review* **2007***, 26*, 1–3.

47. Incropera, F. P.; Dewitt, D. P.; Bergman, T. L.; Lavine, A. S. *Fundamentals of Heat and Mass Transfer, 6th ed.*; Hoboken: John Wiley & Sons, 2007.

48. Kim, M.; Shin, J. Evaporating Heat Transfer of R22 and R410A in horizontal Smooth and Microfin Tubes. *International Journal of Refrigeration* **2005***, 28*, 940–948.

49. Thors, P.; Bogart, J. In-tube Evaporation of HCFC-22 with Enhanced Tubes. *Journal of Enhanced Heat Transfer* **1994***, 1*, 365–377.

50. Yu, M.; Lin, T.; Tseng, C. Heat Transfer and Flow Pattern During Two-phase Flow Boiling of R-134a in Horizontal Smooth and Microfin Tubes. *International Journal of Refrigeration* **2002***, 25*, 789–798.

51. Hatamipour, V.; Akhavan-Behabadi, M. Visual Study on Flow Patterns and Heat Transfer During Convective Boiling Inside Horizontal Smooth and Microfin Tubes. *World Academy of Science, Engineering, and Technology* **2012***, 69*, 700–706.

52. Shedd, T.; Newell, T. Visualization of Two-phase flow Through Microgrooved Tubes for Understanding Enhanced Heat Transfer. *International Journal of Heat and Mass Transfer* **2003***, 46*, 4169–4177.

53. Dang, C.; Haraguchi, N.; Hihara, E. Flow Boiling Heat Transfer of Carbon Dioxide Inside a Small-sized Microfin Tube. *International Journal of Refrigeration* **2012***, 33*, 655–663.

54. Honda, H.; Wang, Y. Theoretical Study of Evaporation Heat Transfer in Horizontal Microfin Tubes: Stratified Flow Model. *International Journal of Heat and Mass Transfer* **2004***, 47*, 3971–3983.

55. Makishi, O.; Honda, H.; Wang, Y. New Theoretical Models of Evaporation Heat Transfer in Horizontal Microfin Tubes. *International Journal of Heat and Mass Transfer* **2006***, 49*, 2328–2336.

56. Koyama, S.; Yu, J.; Momoki, S.; Fujii, T.; Honda, H. Forced Convective Flow Boiling Heat Transfer of Pure Refrigerants Inside a Horizontal Microfin Tube. in *Engineering Foundation Conference on Convective Flow Boiling*, Banff, Canada, 1995.

57. Murata, K. A Correlation for Forced Convective Boiling Heat Transfer of Binary Refrigerant Mixtures: 2nd Report, A Spirally Grooved Tube. *Trans. Jpn. Soc. Mech. Eng. Ser. B* **1996**, *62*, 2732–2728.

58. Thome, J.; Kattan, N.; Favrat, T. Evaporation in Micro-fin Tubes: A Generalized Prediction Model. in *Convective Flow and Pool Boiling Conference*, Kloster, Irsee, 1997.

59. Cavallini, A.; Del Col, D.; Doretti, L.; Longo, G.; Rosetto, L. Refrigerant Vaporization Inside Enhanced Tubes: A Heat Transfer Model. in *Eurotherm Seminar*, Grenoble, France, 1998.

60. Yun, R.; Kim, Y.; Seo, K.; Kim, H. A Generalized Correlation for Evaporation Heat Transfer of Refrigerants in Micro-fin Tubes. *International Journal of Heat and Mass Transfer* **2002**, *45*, 2003–2010.

61. Mori, H.; Yoshida,S.; Koyama,S.; Miyara, A.; Mimoki, S. Prediction of Heat Transfer Coefficients for Refrigerants Flowing in Horizontal Spirally Grooved Evaporator Tubes. in *2002 Japan Society of Refrigerating and Air Conditioning Engineers Annual Conference*, Okayama, Japan, 2002.